Multi-scale Integrated Design and Fabrication of **Ultrathin Broadband Microwave** Absorption Utilizing **Carbon fiber/Prussian blue/Fe_3O_4-based Lossy Lattice Metamaterial**

Yuexuan Li[a], Yugang Duan*[a], Xiaoqing Kang[a]

[a]State Key Lab for Manufacturing Systems Engineering, School of Mechanical Engineering, Xi'an Jiaotong University, Xi'an 710054, China

*Correspondence: ygduan@mail.xjtu.edu.cn

It is obvious that the peak of 2065.48 cm^{-1} and 486.48 cm^{-1} represents the vibration of -CN group and -Fe^{3+}-CN-Fe^{2+} bond for PB (**Fig. S1a)**. The characteristic peak located at 531.31 cm^{-1} suggests the existence of the -Fe-O bond for Fe_3O_4 NPs. After coating with PB, the new vibrational peaks located at 2065.48 cm^{-1} and 492.88 cm^{-1} are attributed to the -C≡N bond and -Fe^{3+}-CN-Fe^{2+} bond, confirming that the successful formation of PB. Moreover, the XRD pattern of Fe_3O_4 NPs (PDF#19-0629), PB ($Fe_4[Fe(CN)_6]_3$, PDF#73-0678) and PB/Fe_3O_4 composite are shown in **Fig. S1b**. It is revealed that two new diffraction peaks of 17.533° and 24.889° in PB/Fe_3O_4 are attributed to the (200) and (220) planes of the PB. It further suggests the presence of PB in PB/Fe_3O_4 nanocomposite.

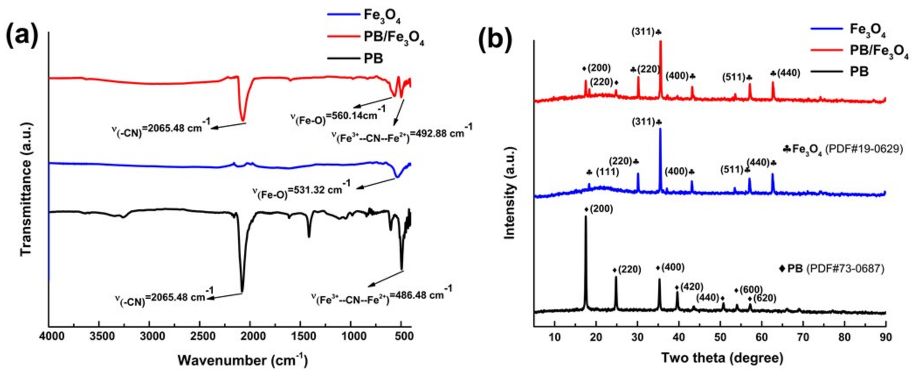

Fig. S1 FT-IR (a) and XRD (a) spectrum of PB/Fe_3O_4 nanocomposite.

Table. 1 Different weight fractions of the SCF/PB/Fe_3O_4/EP composite

Materials	S(10,10)	S(10,20)	S(5,10)	S(5,20)	S(0,20)
SCF (wt%)	10	10	5	5	0
PB/Fe_3O_4 (wt%)	10	20	10	20	20

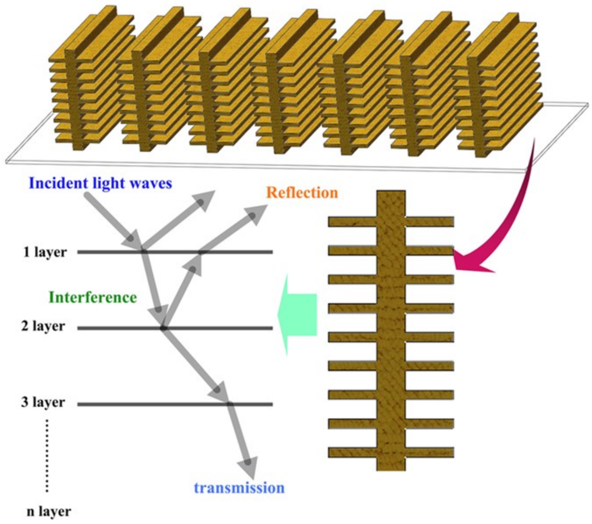

Fig. S2 3D *Morpho*-butterfly scale nanostructure and the colour reflection mechanism.

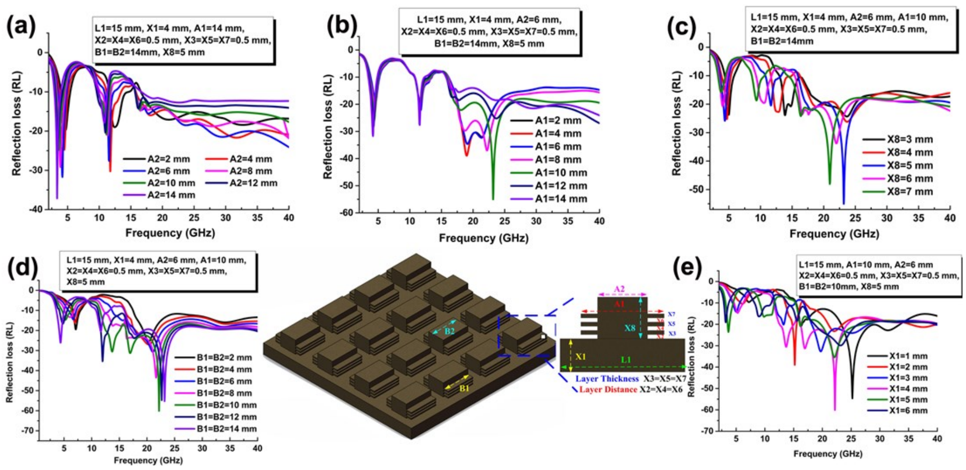

Fig. S3 Optimal parameters of the periodic unit of the BSM absorber.

With an increase in A2, the effect of the microwave absorption frequency is approximately focused on the 5 GHz and 12 GHz. The absorber with A2=14 mm exhibits the strong *RL* ability (RL_{max}=-37.1 dB) in lower frequency point, nevertheless, the absorber of A2=6 mm possesses a broad bandwidth than that of the A2=14 mm (**Fig. S3a**). Moreover, the change of the A1 has a remarkable effect on the microwave absorption performance ranging from 15 GHz to 23 GHz. It is illustrated that the A1=10 mm is an optimal result, exhibiting the maximum *RL* value (RL_{max}=-55 dB) and the broad bandwidth of -26.46 GHz below -10 dB (**Fig. S3b**). Similarly, with increase X8 thickness, the frequency resonance of the BSM absorber has the same trend as those of the A1, as illustrated in **Fig. S3c**. Interestingly, the length of the B1=B2 has a major effect on microwave absorption at the high absorption frequency. **Fig. S3d** displays the optimal microwave absorption bandwidth (*RL*<-9.5 GHz) of 30.32 GHz frequency with B1=B2=10 mm. Moreover, as shown in **Fig. S3e**, there is a maximum absorption peak at the L1 thickness of 4 mm.

Table. 2 Optimized parameters of the periodic unit for the BSM absorber

Parameter	L1	X1	A1	X2	A2	X3	B1	B2	X8	Equivalent plate thickness
Size (mm)	15	4	10	1	6	0.5	10	10	5	5.42

According to the Debye theory, one single semicircle represents once interfacial polarization relaxation processes. The *Cole-Cole* Debye equation between *ε′* and *ε′′* as followed below[1, 2]:

$$\left(\varepsilon' - \frac{\varepsilon_s + \varepsilon_\infty}{2}\right)^2 + \left(\varepsilon''\right)^2 = \left(\frac{\varepsilon_s - \varepsilon_\infty}{2}\right)^2 \qquad (1)$$

Where ε_s and ε_∞ stand for the static dielectric and the relative dielectric at an infinite frequency, respectively.

Moreover, the attenuation constant α is the judgement standard for the microwave absorption performance. Generally, the equation can be expressed as followed[3-5]:

$$\alpha = \frac{\sqrt{2}\pi f}{c} \times \sqrt{\left(\mu''\varepsilon'' - \mu'\varepsilon'\right) + \sqrt{\left(\mu'\varepsilon'' + \mu''\varepsilon'\right)^2 + \left(\mu''\varepsilon'' - \mu'\varepsilon'\right)^2}} \qquad (2)$$

Where *f* is frequency and *c* is the velocity of the light.

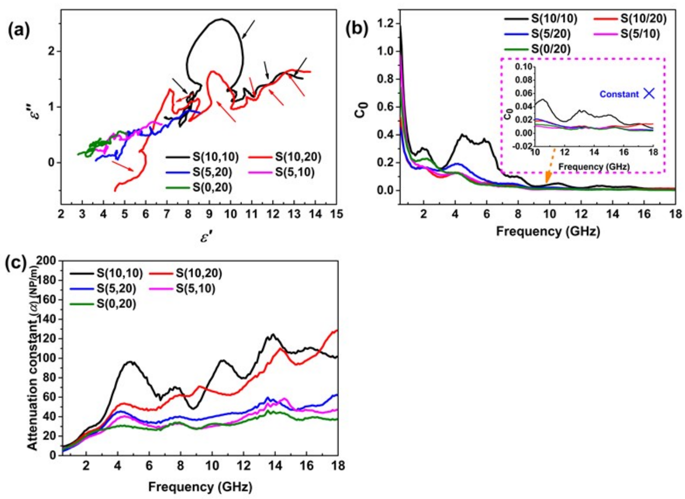

Fig. S4 *Cole-Cole* curves (a), the C_0-*f* curves (b) and the attenuation constant *α*-*f* curves (c) of all the samples.

To further investigate the role of the PB in the complex electromagnetic (EM) absorption process, the SCF/PB/Fe_3O_4/wax and SCF/Fe_3O_4/wax with the SCF(10 wt%), PB/Fe_3O_4 (20wt%), or Fe_3O_4 (20wt%) was fabricated and their EM properties of all samples have exhibited in **Fig. S5**. After Fe_3O_4 encapsulated with PB, the SCF/PB/Fe_3O_4 composite possesses the undesired permittivity (ε' and ε'') values. Based on the free electron theory, $\varepsilon'' \propto 1/2\pi\rho\varepsilon_0 f$, where ρ refers to the resistivity, this indicates that PB-encapsulated SCF/PB/Fe_3O_4 has limited the original conductivity. For the complex permeability, the PB-encapsulated SCF/PB/Fe_3O_4 keeps the better real part of the permeability (μ') at the range of the 6-18 GHz, suggesting that the addition of PB contributes to improving the ability of the magnetic storage. The imaginary apart of the permeability (μ'') have no obvious difference among the SCF/PB/Fe_3O_4 and SCF/Fe_3O_4. (**Fig. S5c-d**). As exhibited in **Fig. S5e-f**, the $tan\delta_\varepsilon$ and $tan\delta_\mu$ values of the SCF/PB/Fe_3O_4 are lower than those of the SCF/Fe_3O_4, illustrating that the slightly lower EM attenuation ability of the SCF/PB/Fe_3O_4 is attributed to the PB-encapsulated Fe_3O_4.

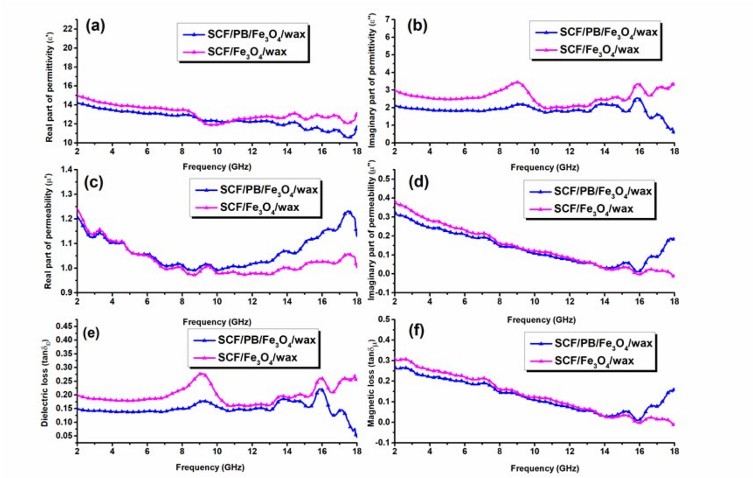

Fig. S5 *Electromagnetic properties of SCF/PB/Fe_3O_4/wax and SCF/Fe_3O_4/wax composite.*

Moreover, as shown in **Fig. S6a**, the PB-encapsulated SCF/PB/Fe_3O_4 composite have more semi-circles than those of SCF/Fe_3O_4, suggesting that PB plays an important role in the enhancement of the polarization relaxation process in the microwave radiation process. Meanwhile, C_0 values of SCF/PB/Fe_3O_4 and SCF/Fe_3O_4 are not a constant, implying that their similarly magnetic loss are attributed to the natural resonance rather than the eddy current effect (**Fig. S6b**). **Fig. S6c** suggests that the attenuation ability of the SCF/PB/Fe_3O_4 gets worse after the addition of PB.

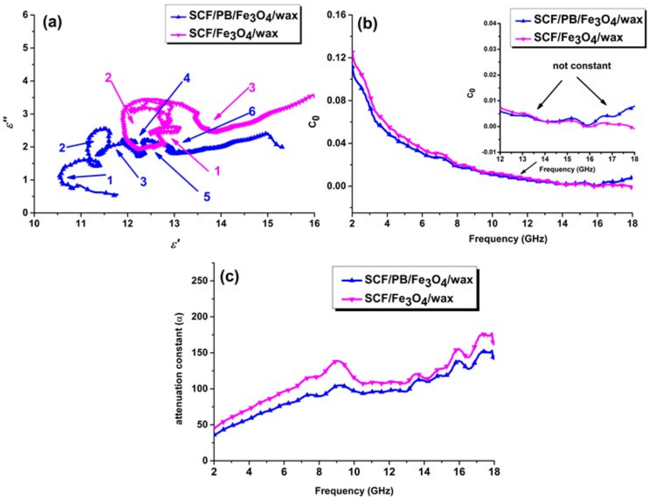

Fig. S6 *Cole-Cole curves (a), the C_0-f curves (b) and the attenuation constant α-f curves (c) of SCF/PB/Fe_3O_4/wax and SCF/Fe_3O_4/wax composite.*

Except for the excellent electromagnetic loss ability, suitable impedance matching is necessary for absorption materials. Here, the impedance matching properties can be expressed in the equation $|Z_r| = \left|\frac{Z_{in}}{Z_0}\right|$, when the $|Z_r|$ is closed to 1, implying that the perfect electromagnetic absorption performance. As shown in **Fig. S7a-b**, the addition of PB is beneficial to optimize the impedance matching. Therefore, the SCF/PB/Fe_3O_4 composite possesses better impedance matching in comparison to the SCF/Fe_3O_4. Thus, the PB-encapsulated SCF/PB/Fe_3O_4 possesses a stronger reflection loss and efficiency bandwidth (**Fig.7Sc-d**).

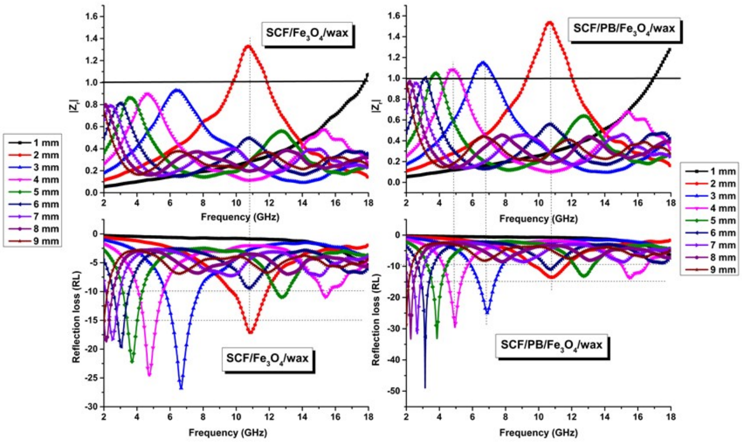

Fig. S7 *The complex impedance matching properties (|Z_r|) (a) and reflection loss (RL) (b) of SCF/PB/Fe_3O_4/wax and SCF/Fe_3O_4/wax composite.*

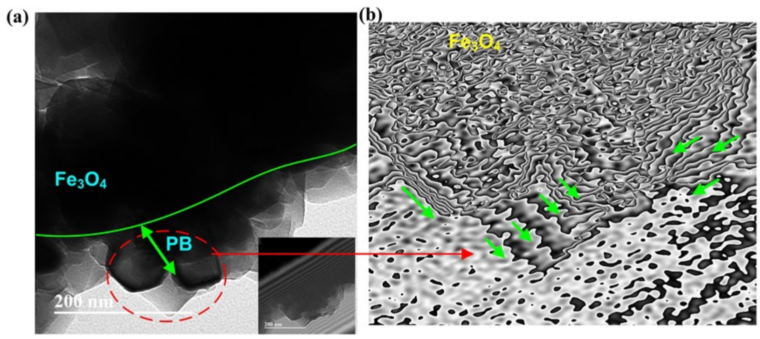

Fig. S8 *TEM image and holograph image (a), the corresponding distribution of magnetic flux lines (b) of PB/Fe_3O_4 nanocomposite.*

Table. 3 Comparison of EMA performance of the previously investigated absorbers.

Absorber type	Filler (wt%)	Absorption	EBD[a] (GHz)	Ref.
Water droplet-based absorber	------	90%	17.6	6
Double split-ring microstructure absorber	------	90.63%	9.43	7
Fe_3O_4@C/rGO-20 absorber	11	90%	6.72	8
GNs/FCIP/epoxy/silicone absorber	72	74.9%	12.6	9
FCIP/Wax	20/60/75[b]	91%	26.85	10
CI/MWCNT/EP/CF/GF	72.744	90%	16.31	11
SCF/PB/Fe_3O_4/EP	30	88.7%	29.54	This work
SCF/PB/Fe_3O_4/EP[c]	30	90%	35	This work

[a]EAB: Effective absorption bandwidth [b]20wt%(1 layer)+60wt%(2 layer)+75wt%(3 layer) [c]TM=50^{o} polarization

Reference

1. X. L. Li, X. W. Yin, H. L. Xu, M. K. Han, M. H. Li, S. Liang, L. F. Cheng and L. T. Zhang, *Acs Appl Mater Inter*, 2018, **10**, 34524-34533.
2. B. Quan, X. H. Liang, X. Zhang, G. Y. Xu, G. B. Ji and Y. W. Du, *Acs Appl Mater Inter*, 2018, **10**, 41535-41543.
3. J. S. Deng, X. Zhang, B. Zhao, Z. Y. Bai, S. M. Wen, S. M. Li, S. Y. Li, J. Yang and R. Zhang, *J Mater Chem C*, 2018, **6**, 7128-7140.
4. H. Pang, W. H. Pang, B. Zhang and N. Ren, *J Mater Chem C*, 2018, **6**, 11722-11730.
5. L. Y. Liang, G. J. Han, Y. Li, B. Zhao, B. Zhou, Y. Z. Feng, J. M. Ma, Y. M. Wang, R. Zhang and C. T. Liu, *Acs Appl Mater Inter*, 2019, **11**, 25399-25409.
6. J. Xie, W. Zhu, I. D. Rukhlenko, F. Xiao, C. He, J. Geng, X. Liang, R. Jin and M. Premaratne, *Opt Express*, 2018, **26**, 5052-5059.
7. S. Li, J. Gao, X. Cao, Z. Zhang, Y. Zheng and C. Zhang, *Opt Express*, 2015, **23**, 3523-3533.
8. H. X. Zhang, Z. R. Jia, A. L. Feng, Z. H. Zhou, L. Chen, C. H. Zhang, X. H. Liu and G. L. Wu, *Compos Part B-Eng*, 2020, **199**.
9. Y. C. Qing, D. D. Min, Y. Y. Zhou, F. Luo and W. C. Zhou, *Carbon*, 2015, **86**, 98-107.
10. S. C. Dang, Y. Lin, X. Z. Wei and H. Ye, *J Mater Sci-Mater El*, 2018, **29**, 17651-17660.
11. Y. X. Huang, X. J. Yuan, M. J. Chen, W. L. Song, J. Chen, Q. F. Fan, L. Q. Tang and D. N. Fang, *Carbon*, 2019, **144**, 449-456.